# Extended Hartmann test based on the pseudoguiding property of a Hartmann mask completed by a phase chessboard

Jérôme Primot and Nicolas Guérineau

We propose to add a specific phase chessboard to the classical Hartmann mask used for wave-front sensing. By doing this we obtain a pseudoguiding of the energy issuing from this mask, allowing for an increase in the sensitivity of the Hartmann test. This property is illustrated by experiment, and a comparison between classical and new Hartmanngrams is presented. © 2000 Optical Society of America

*OCIS codes:* 070.6760, 010.7350, 220.4840, 050.1950.

## 1. Introduction

In 1900 Hartmann proposed a test for optical control that has since been used for a large range of applications.[1] As an example, 100 years after Hartmann's study, the primary mirror of the Zelentchouk giant telescope has been tested during its manufacture with a setup close to that described by Hartmann.[2] The success of this technique is probably due to its simplicity. It uses a mask of holes, usually arranged in a regular square grid, placed in the plane of analysis. These holes break the incoming light into beams, which are deflected according to the local distortions of the sensed wave front. If observed in a plane at a certain distance from the mask, the grid is therefore warped, with the displacement of each spot directly proportional to the local tilt of the wave front and the distance between the mask and the observation plane (see Fig. 1). The sensitivity and the dynamics of this test can thus be adjusted continuously by simple longitudinal translation of the observation plane. Because this operating mode is based on ray tracing, the test is achromatic.

A number of innovative variations to the classical test have been suggested, to adapt it to specific wave-front sensing experiments.[3] For example, Shack proposed replacing the mask of holes with a grid of microlenses.[4] With this modification, all the light coming from the analyzed source is focused at the common focal plane of the microlenses, allowing for better light efficiency. This property is of particular importance for astronomical applications.[5,6] However, the sensitivity is no longer adjustable, since the measurement plane is restricted to the focal plane of the microlenses.

In the classical Hartmann test, although the sensitivity is continuously adjustable, limitations appear when the observation plane is placed far from the mask, owing to diffraction effects. The ray-tracing approach is then no longer valid, and the hole grid is blurred. Our purpose in this paper is to present a new arrangement of the Hartmann test that allows sensitivity for a increase by minimization of blurring effects that are due to diffraction. In Section 2 a description of the classic Hartmann test is presented, issued from a study of the Talbot phenomenon. Then we present the theory of this extended Hartmann test in Section 3. Finally, we conclude this paper in Section 4 by showing experimental results that give what to our knowledge is the first evidence of the ability of this new Hartmann test.

## 2. Hartmann Test and Talbot Interferometer

In the classical description of the Hartmann test diffraction effects are neglected as the observation of the grid of spots is made in a plane close to the mask, as described above. However, for a monochromatic plane wave, self-imaging of the mask can be observed for regularly spaced longitudinal locations of the observation plane, at multiples of $D_T = 2d^2/\lambda$, with $d$ as the pitch of the square grid and $\lambda$ as the wavelength,

The authors are with the Office National d'Etudes et de Recherches Aérospatiales, 29, avenue de la Division Leclerc, 92 322 Châtillon Cedex, France. J. Primot's e-mail address is primot @onera.fr.

Received 29 March 2000; revised manuscript received 11 July 2000.

0003-6935/00/315715-06$15.00/0

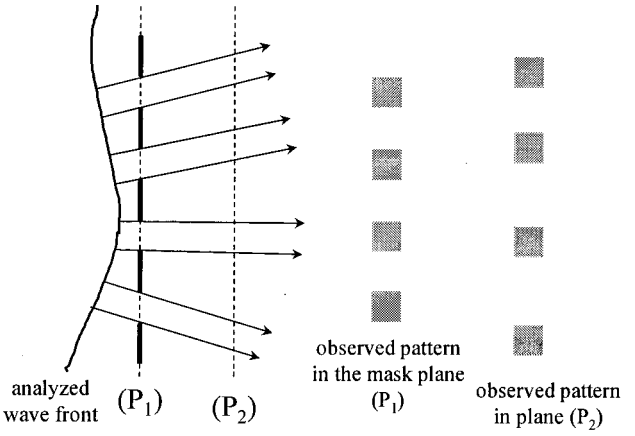


Fig. 1. Principle of the Hartmann test. The distorted wave front is sampled by a grid of square holes. The light beams emerging from the holes are deflected with respect to the local slopes of the wave front.

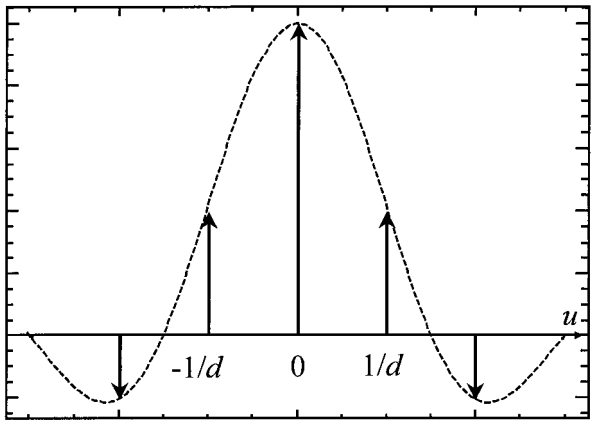


Fig. 2. Orders diffracted by the Hartmann mask (one-dimensional case), for $a = 2d/3$. The main part of the diffracted energy is concentrated in orders −1, 0, and 1.

assuming that the pitch of the mask is large versus the wavelength. This property was first described by Talbot[7] in 1836 and has since been widely studied in the literature.[8] $D_T$ is usually called the Talbot distance. At this distance the observed pattern is not an image in the classical sense, because there is no point-to-point conjugation between the mask and its pseudoimage.

This property of self-imaging can be simply explained. For concision we restrict ourselves to the one-dimensional case and to a plane monochromatic wave. We also consider the Hartmann test to be a grating made of regularly spaced square holes. The transmittance $t(x)$ at the exit of the mask is then given by

$$t(x) = \Pi_a(x) * \mathrm{comb}_d(x), \tag{1}$$

where $a$ is the size of the hole; $\Pi_a(x)$ is the gate function, which is equal to 1 on the $x$ range $[-a/2, a/2]$ and 0 elsewhere; $\mathrm{comb}_d(x)$ is the Dirac comb function of pitch $d$, and $*$ is the convolution product.

The Fourier transform of Eq. (1) yields the series of amplitudes $\mathrm{FT}(u)$ of the diffraction orders:

$$\mathrm{FT}(u) = \frac{\sin(\pi u a)}{\pi u a}\,\mathrm{comb}_{1/d}(u). \tag{2}$$

In most Hartmann tests $a$ is smaller but of the same order as $d$. So the $\sin(x)/x$ function decreases rapidly, and the energy is essentially concentrated in three first orders of diffraction, −1, 0, and 1 (see Fig. 2). Transmittance $t(x)$ of Eq. (1) can then be approximated by

$$t(x) = C_0 + C_1 \exp(2i\pi x/d) + C_{-1} \exp(-2i\pi x/d), \tag{3}$$

where $C_0$ and $C_1 = C_{-1}$ are the amplitudes of the three first diffraction orders.

The zero-order propagates along the axis, and orders −1 and 1 are tilted with respect to the propagation axis by an angle $\theta$ equal to $\lambda/d$. During their propagation, orders −1 and 1 are phase delayed with respect to order 0, owing to the slope of their wave vectors. At the Talbot distance this phase delay is equal to $2\pi$, and the initial state of interference is found. At half the Talbot distance the phase delay is equal to $\pi$, corresponding to a half-period lateral translation. In the vicinity of the mask, phase delays are small, and the global appearance of the mask is not affected; this corresponds to the geometric range of the Hartmann test.

According to this description the Hartmann test in monochromatic light can be seen as a shearing interferometer. The intensity pattern observed in the Talbot plane is the interference of three tilted replicas of the analyzed wave front, which leads to a classical setup belonging to Talbot interferometry (see Ref. 8, p. 62 and references therein).

Figure 3 describes this working mode. The monochromatic analyzed wave front is divided into three replicas, after diffraction by the mask used as a beam splitter. These three replicas constructively interfere at the Talbot distance, leading to a warped self-image of the initial grid. The displacements of the spots are proportional to the local slopes of the wave front.

To synthesize these physical remarks, let us write the interferogram $I(x, z)$ generated at an observation distance $z$ by the mask illuminated by a monochromatic wave under study,

$$E_i(x) = \exp[2i\pi g(x)/\lambda], \tag{4}$$

where $g(x)$ is the optical path introduced by the analyzed wave front. This interferogram is the intensity pattern of the scalar field $E(x, z)$, the sum of three scalar fields diffracted the three components of $t(x)$ given by Eq. (3):

$$E(x, z) = \sum_{p=-1,0,1} C_p \exp\left\{\frac{2i\pi}{\lambda}[x \sin\theta_p + z\cos\theta_p + g(x - z\tan\theta_p)]\right\}, \tag{5}$$

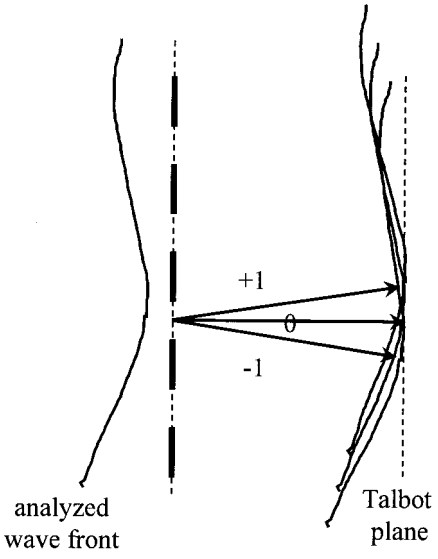


Fig. 3. Hartmann test seen as a lateral shearing interferometer. The observed pattern corresponds essentially to three tilted replicas of the analyzed wave front, which constructively interfere in the Talbot plane.

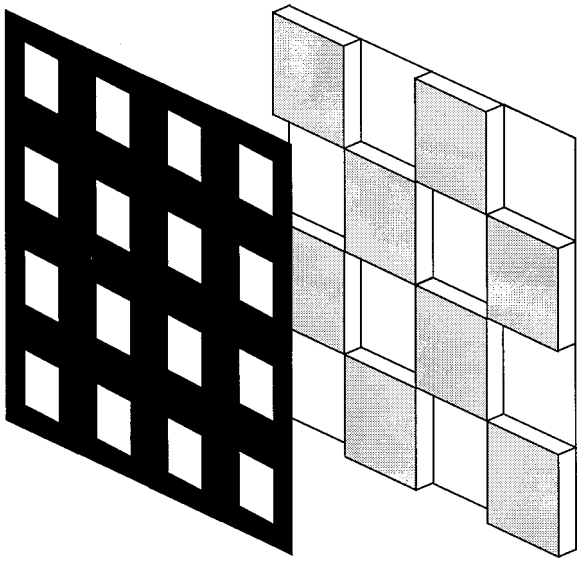

Fig. 4. Addition of the recommended phase chessboard to the Hartmann mask. The height of the phase step is equal to $\pi$ (for the central wavelength).

with $\sin \theta_p = \lambda p/d$. If we assume that $\lambda \ll d$, the expression of $I(x, z)$ reduces to

$$I(x, z) = M_0 + M_1 \cos\left[\frac{2\pi}{d}\left(x - z\frac{\mathrm{d}g}{\mathrm{d}x}\right)\right] + M_2 \cos\left[\frac{4\pi}{d}\left(x - z\frac{\mathrm{d}g}{\mathrm{d}x}\right)\right], \quad (6)$$

where

$$M_0 = {C_0}^2 + 2{C_1}^2, \quad (7)$$

$$M_1 = 4C_0C_1 \cos(\pi\lambda z/d^2), \quad (8)$$

$$M_2 = 2{C_1}^2. \quad (9)$$

From Eq. (6) the analogy with radio-frequency modulation is obvious: In the $z$ plane the modulation of the carrier frequency $2\pi/d$ is proportional to the first derivative of the analyzed wave front with a magnification factor of $z$. So classical numerical demodulation treatments can be processed to extract this derivative information. Because of the Talbot effect that appears in Eq. (8), the contrast $M_2$ of the second term (fundamental harmonic of the interferogram) is cosinusoidal along the $z$ axis of period $d^2/\lambda$. In monochromatic light this contrast is highly degraded at regular distances. In polychromatic light the global contrast $M_2$ of the interferogram, the sum of incoherent intensity patterns, is no longer cosinusoidal along the propagation axis: It is multiplied by a visibility function whose decay increases as the spectral bandwidth enlarges. As a consequence a wave-front analysis based on the use of a Hartmann screen can be processed in two main domains: one corresponding to the usual achromatic Hartmann test, in which ray beam deflections are measured in the vicinity of the mask, and a second domain, in the vicinity of the self-image planes, which is of limited interest, since it requires monochromatic light.

### 3. Extended Hartmann Mask: Theory

Our purpose in this paper is to describe an improvement on the Hartmann test to increase the working domain of the first achromatic operating mode. To do this, we propose complementing the classical square grid of holes with a phase chessboard, as shown in Fig. 4. The pitch of the chessboard is equal to twice the pitch of the mask, and the height of the phase step is equal to $\pi$ for the central wavelength of the spectral band. We will now explain how the operating range can be greatly increased by addition of a $(0, \pi)$ phase chessboard.

As in Section 2, for the sake of simplicity, we restrict ourselves to the one-dimensional case and to a monochromatic plane wave. The transmittance $tp(x)$ of the Hartmann screen completed by a phase chessboard can then be written as

$$tp(x) = \Pi_a(x) * [\mathrm{comb}_d(x)\exp(i\pi x/d)], \quad (10)$$

where the exponential function is introduced to model the alternating phase steps $(0, \pi)$. Then the amplitudes of the diffracted orders are given by

$$\mathrm{FT}p(u) = \frac{\sin(\pi ua)}{\pi ua}[\mathrm{comb}_{1/d}(u) * \delta(u - 1/2d)], \quad (11)$$

where $\delta(u)$ is the Dirac function. We see that the main effect of the phase chessboard is to shift the diffracted orders of $1/2d$, as described in Fig. 5. The energy is now essentially concentrated in two orders, equally tilted at an angle $\theta/2$ with respect to the propagation axis. Because these two preponderant orders take the same phase delay during their prop-

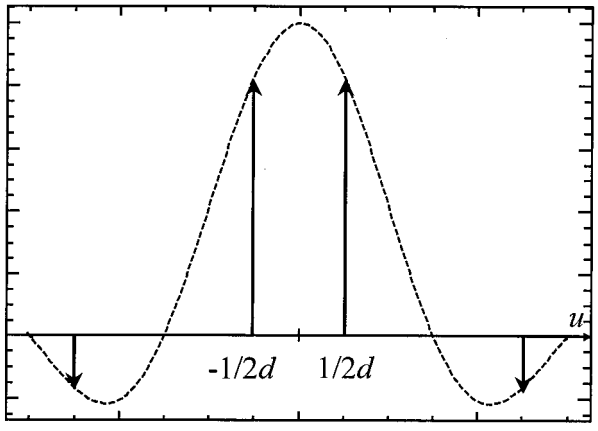


Fig. 5. Orders diffracted by the MHM (one-dimensional case), for $a = 2d/3$. The main part of the energy is now concentrated in the two central orders.

agation, the interferogram observed in a plane is expected to be propagation invariant. To demonstrate this property, the same approach as in Section 2 is used. From the expression of transmittance $tp(x)$ of the modified Hartmann mask (MHM),

$$tp(x) = C_{1/2} \exp(i\pi x/d) + C_{-1/2} \exp(-i\pi x/d), \quad (12)$$

where $C_{1/2} = C_{-1/2}$ are the amplitudes of the two first diffraction orders, we deduce the interferogram $Ip(x, z)$ generated by the mask under aberrant-wave illumination:

$$Ip(x, z) = 2C_{1/2}{}^2\left\{1 + \cos\left[\frac{2\pi}{d}\left(x - z\,\frac{\mathrm{d}g}{\mathrm{d}x}\right)\right]\right\}. \quad (13)$$

An important point highlighted by Eq. (13) is that the contrast of the interferogram is propagation invariant and achromatic, allowing for analysis of the interferogram in polychromatic light and in any observation plane. At a practical stage the obtained transmittance diffracts more than two orders and residual fluctuations of the contrast are expected along the propagation axis.

Nevertheless, one remarkable case is obtained when $a = 2d/3$. When this condition is fulfilled, it can be shown that a new self-imaging plane appears at $D_T/6$, where $D_T$ is the Talbot distance of the mask alone, and at every multiple of this distance. To illustrate this property, we calculated the intensity $I(x, z)$ of the diffracted field for two cases, using the approach of the angular spectrum of plane waves.[9] In the first case we consider the Hartmann mask of period $d$ that generates a self-image at the Talbot distance $D_T$. In Fig. 6(a) the intensity of the propagated field is shown as gray levels, between $z = 0$ and $z = D_T$ planes. At fractional Talbot distances classical results can be observed. For example, at half the Talbot distance, the original intensity pattern is reproduced but shifted by half a period $d$; at $D_T/4$ global contrast is largely decreased.

In the second case we consider the MHM. The calculated intensity of the propagated field is shown in Fig. 6(b) in the same $z$ range as in 6(a). This figure highlights the formation of self-images at regular distances multiple of $D_T/6$. Moreover, at any distance $z$, we can observe that an interferogram appears with a good contrast. This contrast is nearly propagation invariant in opposition to the first case in which strong variations appeared, as if the energy emerging from the holes were guided through square pipes. In fact, this is only a guiding of the global energy: There is no point-to-point correspondence between the observed images of the square grid for two different longitudinal locations.

Under polychromatic illumination, this property remains, but with a lesser quality, since the phase

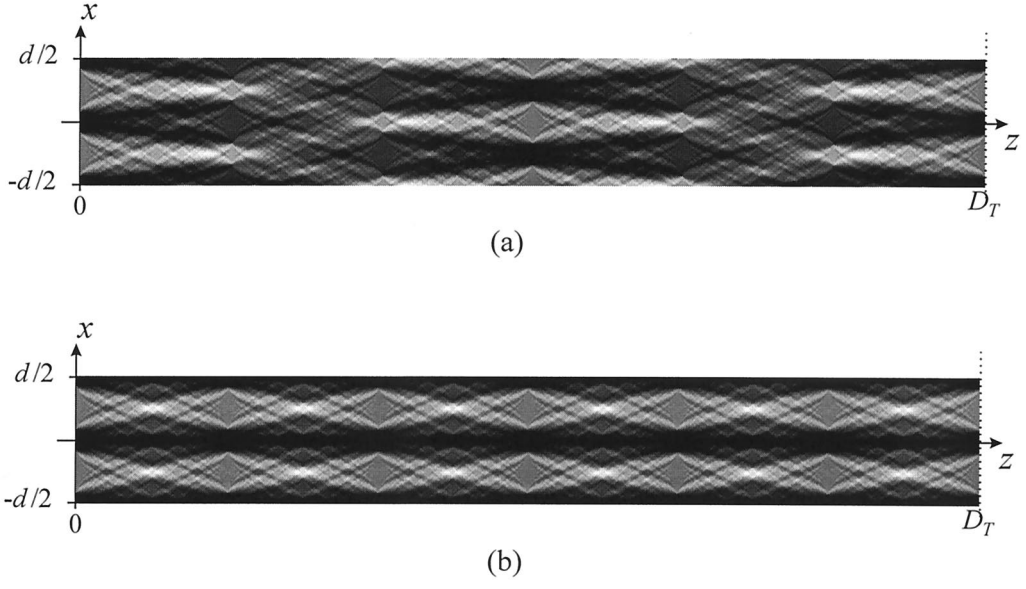


Fig. 6. Numerically calculated intensity for the propagation of the optical field diffracted by the Hartmann mask (a) without and (b) with phase chessboard, between $z = 0$ and the first Talbot distance $D_T$ of the Hartmann mask (in monochromatic illumination).

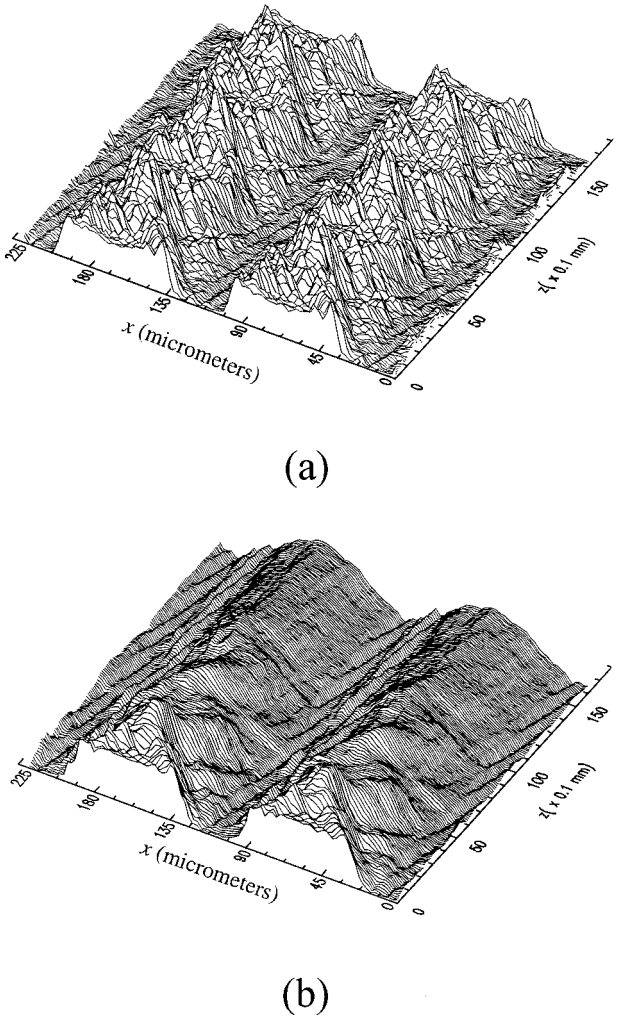


Fig. 7. Experimental evolution of two cells of the recorded interferogram along the propagation axis $z$ produced by the MHM under (a) laser illumination and (b) white-light illumination.

step is no longer strictly equal to $\pi$. Thus we expect to reduce the blurring effect that is due to diffraction by adding a phase chessboard and thereby increase the sensitivity of the Hartmann test.

## 4. Experimental Study

A MHM as described in Section 3 has been realized. The mask is a grid (pitch $d = 100$ $\mu$m) of square holes (opening, 66 $\mu$m). The phase chessboard has a pitch of 200 $\mu$m, and the height of the phase step is equal to $\lambda_0/2$ with $\lambda_0 = 0.633$ $\mu$m. For these values the Talbot distance is 31.6 mm. This MHM was studied under coherent and white-light illumination to verify the pseudo-guiding effect of the diffracted field. Then a Hartmann test was processed under white-light illumination, and Hartmanngrams were recorded.

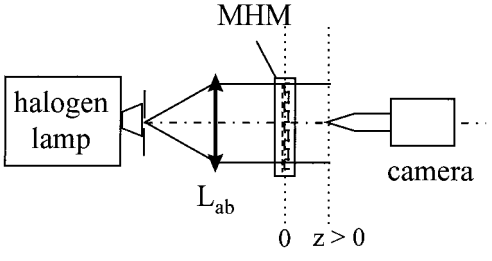


Fig. 8. Use of the MHM as a wave-front sensor. Optical setup.

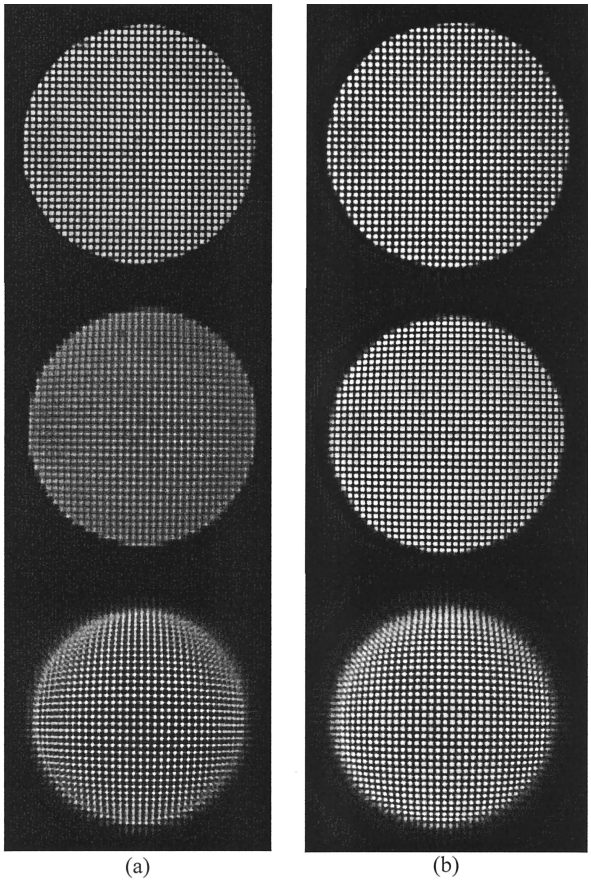


Fig. 9. Hartmanngrams obtained for a spherical aberration at increasing distances (from top to bottom: $z = 0$, 5.3, and 15.8 mm) from the Hartmann mask (a) without and (b) with phase chessboard.

### A. Coherent Illumination

A He–Ne laser illuminates a pinhole of diameter 10 $\mu$m at the focal plane of a collimating lens of focal length 450 mm. Images are grabbed with a CCD camera mounted with a microscope objective; 160 images were recorded corresponding to different $z$ values, from $z = 0$ to $z = 16$ mm ($\approx D_T/2$) with a translation step of 0.1 mm. Figure 7(a) shows the evolution of the responses delivered by a line of 100 pixels across a propagation-distance range of 16 mm. We verify that self-images appear at regular distances, multiples of 5 mm ($\approx D_T/6$), and that the contrast of the intensity profile is quasi propagation invariant.

### B. White-Light Illumination

A halogen lamp illuminates a pinhole of diameter 80 μm at the focal plane of the same collimating lens. The spectral range of the camera is [0.5, 0.9 μm]. Figure 7(b) shows the evolution of the responses delivered by the same line of 100 pixels. We observe that the white-light interferogram exhibits a sinusoidal modulation when the observation distance is increased. An important point highlighted by this experimental study is that the MHM, under white-light illumination, produces a quasi-sinusoidal interferogram.

### C. Application to Wave-Front Sensing

To illustrate the interesting property of the MHM, we performed a simple wave-front sensing experiment. The optical setup is illustrated in Fig. 8. A pinhole of diameter 80 μm illuminated by a halogen lamp is placed at the focus of a spherical lens generating a plane wave front with a large spherical aberration. In Fig. 9 we show images delivered by the sensor at several distances from the mask (a) without and (b) with phase chessboard. Note the increasing distortion of these Hartmanngrams, characteristic of the spherical aberration. In the first configuration we observe that the contrast of the Hartmanngrams depends on the working distance, and, at a given distance, this contrast is not uniform (see the bottom image, at $z = 15.8$ mm). It can be shown that these fluctuations are mainly due to the diffraction order 0 of the Hartmann mask that makes the intensity distribution in an observation plane dependent on the second-order derivative term of the analyzed wave front (see Ref. 8, pp. 63–64). For example, at $z = 5.3$ mm, the contrast is largely decreased, and the Hartmanngram is no longer exploitable. In the recommended configuration (b) we note a clear qualitative improvement of the intensity distribution of the modified Hartmanngrams at any observation distance.

## 5. Conclusion

In this paper we have presented a way to increase the sensitivity of the Hartmann test by addition of a phase chessboard. By properly choosing the ratio between the size of the square holes and the pitch of the mask we can reduce the self-imaging distance by a factor of 6. In this case we have shown that the global energy issuing from the mask is pseudoguided in square pipes and that this property is still verified in polychromatic light. This new setup has evident applications in wave-front sensing problems, which will be tested in the near future. However, it is probably also of interest for other kinds of problems in optical metrology.

## References


1. I. Ghozeil, "Hartmann and other screen tests," in *Optical Shop Testing*, D. Malacara, ed. (Wiley, New York, 1992), pp. 367–396.
2. A. Zverev, S. A. Rodioniv, M. N. Sokolskii, and V. V. Usoskin, "Mathematical principles of Hartmann test of the primary mirror of the Large Azimuthal Telescope," Sov. J. Opt. Technol. **44,** 78–81 (1977).
3. F. Roddier, "Variations on a Hartmann theme," Opt. Eng. **29,** 1239–1242 (1990).
4. R. V. Shack and B. C. Platt, "Production and use of a lenticular Hartmann screen (abstract)," J. Opt. Soc. Am. **61,** 656 (1971).
5. F. Merkle, "Adaptive optics," in *International Trends in Optics* (Academic, New York, 1991).
6. J. Primot, G. Rousset, and J. C. Fontanella, "Deconvolution from wave-front sensing: a new technique for compensating turbulence-degraded images," J. Opt. Soc. Am. A **7,** 1589–1608 (1990).
7. F. Talbot, "Facts relating to optical science. IV," Philos. Mag. **9,** 401–407 (1836).
8. K. Patorski, "The self-imaging phenomenon and its applications," in *Progress in Optics*, E. Wolf, ed. (North-Holland, Amsterdam, 1989), Vol. 27, pp. 1–108.
9. R. F. Edgar, "The Fresnel diffraction images of periodic structures," Opt. Acta **16,** 281–287 (1969).